Available online at www.sciencedirect.com
SCIENCE DIRECT®
Robotics and Autonomous Systems 50 (2005) 177–194
Robotics and Autonomous Systems
www.elsevier.com/locate/robot

Optic flow regulation: the key to aircraft automatic guidance

Franck Ruffier*, Nicolas Franceschini

Biorobotic research group, Movement and Perception Lab., CNRS/Univ. de la Méditerranée, 31, chemin Joseph Aiguier, 13402 Marseille Cedex 20, France

Received 6 September 2004; accepted 9 September 2004
Available online 25 December 2004

Abstract

We have developed a visually based autopilot which is able to make an air vehicle automatically take off, cruise and land, while reacting appropriately to wind disturbances (head wind and tail wind). This autopilot consists of a visual control system that adjusts the thrust so as to keep the downward optic flow (OF) at a constant value. This autopilot is therefore based on an *optic flow regulation loop*. It makes use of a sensor, which is known as an *elementary motion detector* (EMD). The functional structure of this EMD was inspired by that of the housefly, which was previously investigated at our Laboratory by performing electrophysiological recordings while applying optical microstimuli to single photoreceptor cells of the insect's compound eye.

We built a proof-of-concept, tethered rotorcraft that circles indoors over an environment composed of contrasting features randomly arranged on the floor. The autopilot, which we have called OCTAVE (Optic flow based Control sysTem for Aerial VEhicles), enables this miniature (100 g) rotorcraft to carry out complex tasks such as ground avoidance and terrain following, to control risky maneuvers such as automatic take off and automatic landing, and to respond appropriately to wind disturbances. A single visuomotor control loop suffices to perform all these reputedly demanding tasks. As the electronic processing system required is extremely light-weight (only a few grams), it can be mounted on-board micro-air vehicles (MAVs) as well as larger unmanned air vehicles (UAVs) or even submarines and autonomous underwater vehicles (AUVs). But the OCTAVE autopilot could also provide guidance and/or warning signals to prevent the pilots of manned aircraft from colliding with shallow terrain, for example.

Keywords: Unmanned aerial vehicles; Automatic flight control system; Micro-air vehicles; Optical flow; Motion detector; Biorobotics; Biomimetics; Bionics

1. Introduction

The biorobotics approach developed at our laboratory since 1985 [13,25–27,30,33–37,43,44] has led to designing and testing robots which process similar cues to those used by insects in real life. When building autonomous flying machines weighing less than 100 g, taking a look at natural autonomous fliers such as birds, chiroptera and winged insects can suggest some

Abbreviations: UAV, unmanned aerial vehicles; MAV, micro-air vehicles; AFCS, automatic flight control system; AUV, autonomous underwater vehicles; OF, optical flow; EMD, elementary motion detector

* Corresponding author. Tel.: +33 4 91 16 45 38; fax: +33 4 91 16 45 83.
E-mail addresses: ruffier@laps.univ-mrs.fr (F. Ruffier), franceschini@laps.univ-mrs.fr (N. Franceschini).

0921-8890/$ – see front matter © 2004 Elsevier B.V. All rights reserved.
doi:10.1016/j.robot.2004.09.016

interesting solutions to the problems arising on this tiny scale. Some winged insects were solving obstacle avoidance, odometry and navigation problems several hundred million years before there were any humans on Earth, and their efficient guidance principles can provide robotics with innovative and well tested ideas. Winged insects have been known for 65 years to react visually to the relative movement of the ground caused by their own bodily motion [21]. Surprisingly, this natural visual cue, which has later been called the "*optic flow*" (OF), has not pervaded the field of aerospace engineering yet, although many data have been gleaned about the sensors and circuits that process the OF in the insect eye [8,14,18,31].

Conferring some autonomy and authority on an aircraft, especially during take off and landing and in the presence of wind disturbances, is a challenging task. It involves many parameters such as the mass, on-board energy and on-board processing resources required. Some of these issues have been addressed in the case of large UAVs and drones using conventional computer vision systems (e.g., [2,15,20,32,38,39]). One particularly remarkable example is the R50 Yamaha helicopter automated by Amidi et al., which performed all its maneuvers (even the riskiest ones, such as hovering and landing) on the basis of natural visual landmarks and accurate sensor fusion [2]. Because of the heavy equipment required on-board this rotorcraft, the total airborne mass amounted to 67,000 g. Building 1000 times lighter UAVs (in the 100-g range) or 1 million times lighter UAVs (in the insect range) may require taking a different approach to the control systems, as several authors have attempted to do by turning to long-existing biological systems [5–7,16,19,25–28,33–37,40,43–45]. Insect based visual flight control simulations have shown how useful the OF can be for autonomous navigation purposes [25,26,28]. Based on their own detailed behavioural studies on honeybees' grazing landings, Srinivasan et al. proposed a landing strategy that consisted in maintaining a constant OF [41]. Two requirements were then defined: (i) maintaining a constant descent angle, (ii) adjusting the forward flight speed so as to maintain a constant image angular velocity throughout the descent [40]. The authors fulfilled these two requirements on a robotic gantry without any dynamics [40]. More recently, Chahl et al. attempted to satisfy the above two requirements on a free-flying model aircraft when controlling its descent from an altitude of 60 m down to 30 m [6]. Ichikawa et al. addressed the problem of hovering with a 100-g model helicopter using a basic motion detection device [19]. Altitude control and obstacle avoidance systems have also been tested qualitatively on a free flying model plane [5,16].

At our laboratory, we have long regarded winged insects as valuable model systems for building dynamic stabilization and visual guidance abilities into artificial micro-flyers [25]. In 1986, Franceschini et al. designed an optronic angular velocity sensor [3,12], the principle of which was based on the findings these authors had made on fly EMDs by performing electrophysiological recordings on single neurons while concomitantly applying optical microstimuli to two photoreceptor cells within a single ommatidium [14]. This velocity sensor developed into a small (6 g) analog circuit [4] was used in particular onboard the fast obstacle-avoiding "robot mouche" (robofly) [4,13]. Recently, we designed a lighter (0.8 g) version of this EMD circuit, in which analog and digital devices are combined [36]. In the mid-1990's, a similar principle was used again, independently, to design a smart VLSI circuit called the "facilitate and sample" velocity sensor [23]. In 1994, the Laboratory's first OF-based altitude control simulation studies were published [25]. Netter and Franceschini simulated OF-based terrain following behaviour [26,27] with a forward looking 20 pixel-retina (the validity of the latter simulation was recently confirmed using a similar eye, looking down in the same way, over a similar environment [45]). These authors also established that OF-based landing could be achieved by linearly decreasing the rotorcraft's forward speed while maintaining a reference OF value [26]. They constructed a tethered 850 g helicopter which was able to hop over obstacles on the basis of its 19 EMDs [27]. The biologically inspired microrobotics approach has also led to the development of a new EMD-based visual sensor called OSCAR, which enables a 100 g tethered MAV to robustly perform tasks such as visual fixation and tracking, even in the presence of various disturbances [37,43,44].

In a previous paper [34], we described a tethered rotorcraft capable of effective terrain following, equipped with a simple, vision-based automatic flight control system (AFCS). We showed that the AFCS, called OCTAVE (Optic flow based Control sysTem for Aerospace VEhicles), enabled a minimalistic optronic

system to guide an aerial vehicle automatically on the basis of visual cues, without any need for a remote pilot to carry out ground avoidance tasks. The remote pilot (or an onboard system having some authority) was simply required to set: (i) a pitch angle and (ii) an OF set point. These two parameters determined the height at which the robot flew above the ground in the absence of wind disturbances. At a given OF reference, any change in the ground speed occurring for any reason whatever automatically led the aircraft to ascend or descend.

The present results enable autonomous aerial robots to perform three further reputedly difficult tasks: autonomous take off, autonomous landing and autonomous compensation for wind disturbances. In Section 2, we describe the insect based visual guidance principle adopted. Section 3 focuses on the experimental setup used to test this principle on a tethered Micro-Air Vehicle. In Section 4, we describe the autonomous terrain following, autonomous take off, autonomous landing and autonomous flight performances of the aircraft with the presence of wind disturbances. In Section 5, we show that the balance between ground speed and height in an air vehicle equipped with the OCTAVE autopilot will depend suitably on the vertical wind speed profile.

2. Visual guidance strategy

2.1. Optic flow (OF) under pure translation over a terrain

An eye-bearing MAV flying in pure translation along the x-axis over an unknown terrain (Fig. 1a) generates an elementary translational OF, ω:

$$\omega = \frac{v_x}{D} \sin \Phi \tag{1}$$

where v_x is the speed (ground speed) of the aircraft with respect to the ground, D its distance from the ground and Φ the angle between the gaze direction and the horizontal heading direction.

The OF generated is very small around the direction of self-motion ($\Phi = 0^\circ$), which is a pole of the OF field. The largest OF occurs at an angle $\Phi = 90^\circ$ from the pole. As we will see later, we keep the robot's eye oriented downwards ($\Phi = 90^\circ$) so that D becomes the local height h with respect to the ground (Fig. 1b). Under these conditions, the OF range is maximized and ω is simply the ratio between the ground speed v_x and the height h.

$$\omega = \frac{v_x}{h}, \Phi = 90^\circ \tag{2}$$

2.2. Visual guidance in the "longitudinal plane"

Interestingly, the vertical plane (x, z) defined by Fig. 1 is the most relevant plane for a sighted aircraft, a bird or an insect that has to move from point A to point B (Fig. 2). Its three-dimensional trajectory defines a succession of piecewise vertical planes with its vertical projection on the ground (i.e., the track). On the other hand, the track is the region of interest where the

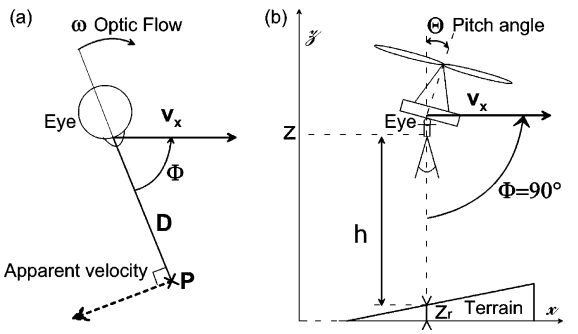

Fig. 1. (a) An eye translating at velocity v_x over a contrast point P located at distance D and elevation Φ generates an angular retinal velocity ω, the local optic flow (OF), as described by Eq. (1). (b) A rotorcraft pitched forward by an angle Θ flies at groundspeed v_x in the absence of wind. If the gaze direction is maintained vertically downwards ($\Phi = 90^\circ$) by some means, D becomes h, the distance above the terrain.

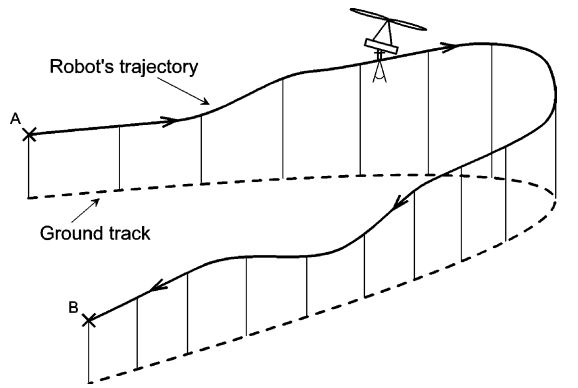

Fig. 2. The bold line describes the 3D trajectory of a rotorcraft and the dotted line the ground track.

ventral eye described in Fig. 1b can discover contrasting features. The presentation and the discussion of the OCTAVE autopilot will be restricted to this longitudinal plane. When traveling from A to B, the rotorcraft (Fig. 2b) is assumed to keep its body oriented in the longitudinal plane defined locally by the trajectory and the ground track. Both the rotorcraft's body and the rotorcraft's eye are adjustable within this longitudinal plane and we assume there is no degree of freedom for roll.

2.3. Insects and rotorcraft

The guidance strategy proposed here is inspired by observations made by Kennedy more than 50 years ago on the flight behaviour of mosquitoes [21] and migrating locusts [22]. This author summarized his *optomotor theory* as follows: "any image movement over the ventral ommatidia which diverges from the preferred velocity [. . .] evokes compensatory responses" [22]. In a similar vein, "visual control of flight speed [of a bee flying through a tunnel] is achieved by monitoring and regulating the apparent motion of the [lateral] visual panorama" [41]. Upon analyzing the flight of the free-flying fruitfly (*Drosophila*), David noted the existence of a relationship between flight speed and body angle [10]. The direction of the thrust generated by the two wings is mainly governed by the body pitch angle. The horizontal component of the thrust (i.e., the propulsive force, which causes the forward motion and determines the flight speed) therefore depends on the body pitch angle as well. Pitch angle and thrust are also the sole parameters in the OCTAVE autopilot that guides our miniature rotorcraft. The thrust vectoring mode we use, which consists in acting only on the direction (body pitch angle) and the magnitude of the rotorcraft's thrust vector, is therefore comparable to the propulsion mode used by the fruitfly.

2.4. OCTAVE visuomotor control loop

The OCTAVE Automatic Flight Control System (AFCS) that we propose consists in an *optic flow regulator* that controls the thrust (Fig. 3). This autopilot differs fundamentally from other AFCS classically used in aerospace research, such as those based on pressure altitude servoing (by means of a barometric sensor), ground height servoing (by means of a radio-altimeter sensor, for instance) or ground speed servoing (by means of a Doppler radar, for instance). In essence, the OCTAVE AFCS estimates neither the ground height h nor the ground speed v_x but only the ratio between

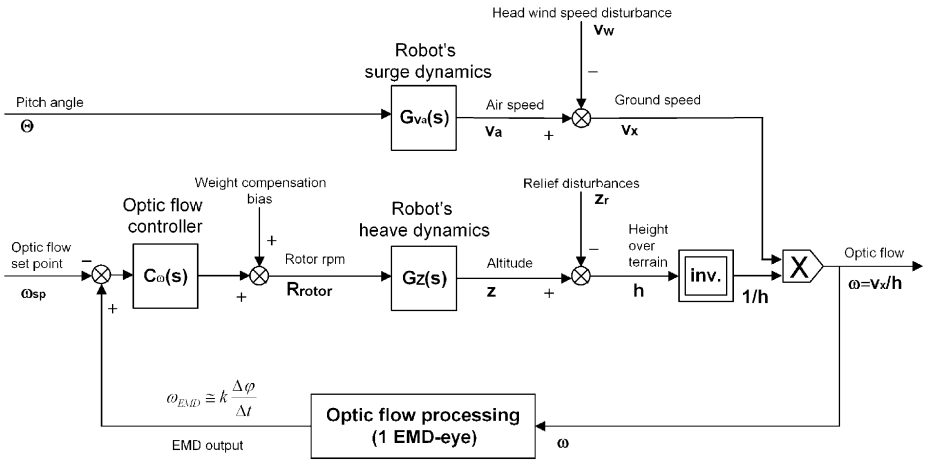

Fig. 3. The OCTAVE autopilot controls two inputs on the robot's dynamics. First the pitch angle Θ of the craft determines the *direction of the thrust vector*, which will eventually determine the groundspeed v_x. Secondly, the *amplitude of the thrust vector*, which will eventually determine the altitude z. In the results presented in this paper, the thrust direction is set at a constant value while the thrust magnitude results from the OF regulation. The OF controller $C_\omega(s)$ which we incorporated into the loop regulates the OF ω, which is measured by an EMD circuit. When the EMD output ω_{EMD} (V) is greater than the OF set point ω_{sp}, $C_\omega(s)$ commands a greater rotor speed (*rpm*). This leads to an increase in the altitude (via the heave dynamics), which results in a decrease in the OF. The ground speed v_x which depends on the rotorcraft's pitch angle, can be said to weight the OF according to Eq. (2).

the two variables, which is the OF (Eq. (2)). The robot then reacts to the error signal in OF by changing its *thrust* via the rotor speed (rotations per minute, *rpm*). Any increase in the OF (due to a decrease in the height h above the ground or to an increase of ground speed v_x) causes the rotor *rpm* to increase (see the signs of the signals on the comparator, Fig. 3, left), until a height h over ground is reached, which re-establishes the requisite OF.

Output disturbances of two kinds can affect the "OCTAVE" visuomotor loop:

1. The wind speed v_w which adds to the airspeed (in case of a tail wind) or subtracts from the airspeed (in case of a head wind), giving the groundspeed v_x.

$$v_x = v_a - v_w \tag{3}$$

2. The local relief altitude z_r which is subtracted from the absolute aircraft altitude, resulting in the height h over the ground.

$$h = z - z_r \tag{4}$$

Both the relief and the wind speed are treated like "disturbances" affecting the OF (Fig. 3). A rising relief or a stronger tail wind will both immediately increase the OF estimate ω_{EMD}, and hence the error signal and the thrust, and will thus raise the aerial robot above the ground until the OF estimate ω has decreased close to the OF set point.

The visual control system described in Fig. 3 is a simplified description of the complex dynamics of the visuomotor plus aero-mechanical processes at work. In our analysis of the visuomotor control loop, we focused on the surge and heave dynamics.

There are two main parameters to the OCTAVE autopilot (Fig. 3):

1) The robot's pitch angle Θ (Figs. 1 and 2), which determines the direction of the rotor thrust.The horizontal component of the thrust determines the air speed. By keeping the robot's pitch constant, without the presence of any wind, the ground speed v_x remains constant, and the visuomotor control loop will thus interpret any changes in the OF as if they were changes in the height h over the ground.
2) The OF set point, ω_{sp}. This parameter defines the ratio between the ground speed v_x and the height h above the ground (Eq. (2)).

2.5. OCTAVE control loop implementation

The transfer function $G_{Va}(s)$ gives the surge dynamics between the pitch angle Θ (°) and the air speed v_a (m/s). The heave dynamics transfer function $G_z(s)$ gives the heave dynamics, the linear transfer between the rotor speed R_{rotor} (rpm) around the operating point and the altitude, z (m). $G_z(s)$ was identified under the present experimental conditions from the response to a rotor *rpm* step.

$$\begin{aligned} G_z(s) &= \frac{Z(s)}{R_{rotor}(s)} = \frac{K_z \times \omega_z^2}{s^2 + 2\xi_z\omega_z s + \omega_z^2} \quad \text{with} \\ K_z &= 0.00512\,(\text{m/rpm}),\ \xi_z = 0.223, \\ \omega_z &= 0.951\,\text{rad/s} \end{aligned} \tag{5}$$

A lead controller $C_\omega(s)$ was introduced into the feedback loop to increase the phase margin and the damping, thus improving the stability of the loop and decreasing the response overshoot. The controller also includes a low-pass filter, which reduces the effects of short time errors on the OF estimation and smoothes the jumpy control signal whenever a new OF measurement is made. This low-pass filter suitably decreases the jitter in the rotor control signal. The overall OF controller $C_\omega(s)$, which runs on-line on a dSpace DSP board, is:

$$\begin{aligned} C_\omega(s) &= K_C \left(\frac{\tau_1 s + 1}{\tau_2 s + 1}\right)\left(\frac{1}{\tau_3 s + 1}\right) \quad \text{with} \\ K_C &= 180\,(\text{rpm/V}), \quad \tau_1 = 1.5\text{s}, \\ \tau_2 &= 0.12\,\text{s}, \quad \tau_3 = 0.05\,\text{s} \end{aligned} \tag{6}$$

Since the system actually includes various aeromechanical "couplings", we checked that the controller is robust to parametric variations in the 1–3 m/s ground speed range and in the 0–2 m altitude range in the absence of any wind disturbances. The gain K_z was found to depend in a ±50% range on both the rotor control signal (increasingly) and the speed (decreasingly). The pulsation ω_z and the damping factor ξ_z vary to a lesser extent. We neglected the coupling between the rotor speed, R_{rotor} (*rpm*), and the airspeed, v_a (m/s): our experimental data showed that this coupling is weak (the speed remains fairly constant, see Fig. 8b).

Fig. 4. Microcontroller-based EMD circuit with its lens. One face of the 400 μm-thick PCB (size: 20 mm × 27 mm, mass: 0.8 g) includes the lens (focal length: 8.5 mm) mounted in front of two matched PIN-photodiodes. The reverse side of the PCB (right) incorporates the μC-based EMD circuit [36].

A local rotor speed control loop (not shown in Fig. 3) was implemented to improve the dynamic properties of the overall visuomotor control system. This control loop counteracts any local aerodynamic disturbances impinging on the rotor (90% of the disturbance is rejected in 50 ms). At low rotor control signal values, the MAV stays at altitude zero until a lift threshold is reached that equals its weight. This "dead zone" is compensated for by adding a bias to the rotor control signal (see Fig. 3).

For the sake of convenience, the control system is hosted by an I/O DSP board (see Section 3B). The control system is composed of a few digital filters and summation elements and runs at 1 kHz. Thanks to the great simplicity of this control system, it can be implemented on-board a tiny 8-bit microcontroller.

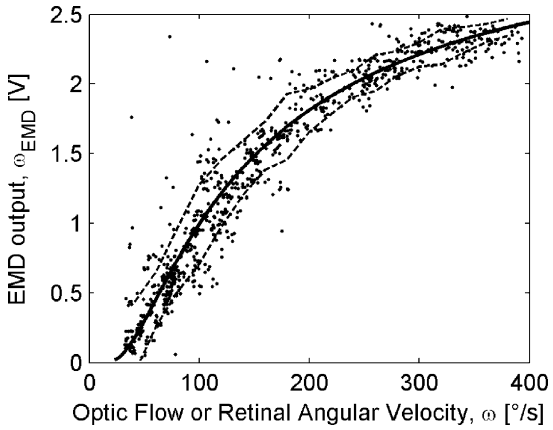

Fig. 5. Microcontroller-based EMD output (in Volts) versus angular velocity. This figure shows the EMD response to 863 motion stimuli at various angular speeds. These data were collected using the textured ground presented in Fig. 7b, which shows various contrasting edges and bars with a relatively low contrast m ($0.04 < m < 0.3$) (See Eq. (8)). The EMD circuit's mean response (bold solid line) are monotonic with respect to the angular velocity. The experimental data are clustered around the mean response with a standard deviation of ±0.16 V (dotted profiles). This value is comparable to the standard deviation measured on Harrison and Koch's (correlation-based) VLSI EMD circuit [17].

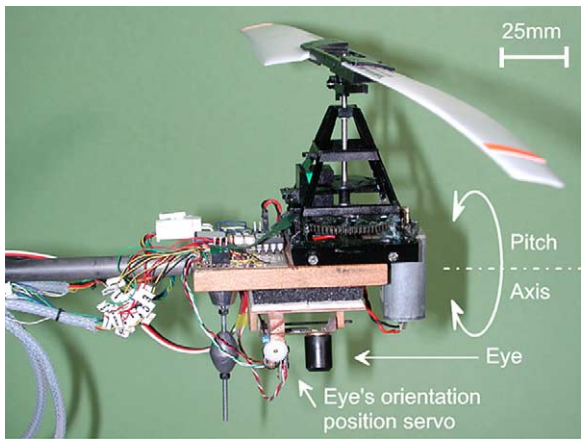

Fig. 6. A 100 g sighted rotorcraft developed for testing the OF autopilot. A PWM-controlled DC motor drives the 30 cm diameter, 5 g rotor via a reducer. The robot can be oriented around its pitch axis by means of an external signal. The electronic eye is mounted on a thin board, the pitch of which is controlled by a 2.4 g position servo system. When the robot's pitch angle is changed by the experimenter, the micro-servo counter-rotates the eye so as to keep the gaze oriented vertically downwards, as shown in Figs.1b and 2.

2.6. Bio-inspired OF processing

The OF processing is carried out by two devices:

1) An elementary eye, which transforms the optic flow ω generated by the robot's forward motion into a time lag Δt between the responses of two neighboring photoreceptors: Δt is an inverse function of ω (Eq. (7)). The two photoreceptor optical axes are separated by an angle $\Delta\varphi$.
2) An insect-based elementary motion detector (EMD), which processes this time lag Δt in a nonlinear way to provide the OF estimate ω_{EMD} (V) according to:

$$\omega_{\mathrm{EMD}} \cong k\frac{\Delta\varphi}{\Delta t} = k'\omega \tag{7}$$

Our current hybrid implementation of an EMD, which combines both analog preprocessing and digital microcontroller-based processing, is a small module weighing only 0.8 g [36], which lends itself easily to being mounted on-board the aerial robot (Fig. 4).

The responses of this velocity sensor are monotonic with respect to the angular velocities in a 10-fold range (from 40 to 400°/s) (Fig. 5). The curve is not linear because a long-lived decaying function converts Δt into the EMD circuit's output signal. The optic flow is therefore measured with a better sensitivity at low angular speeds (under 150°/s) than at high angular speeds (over 250°/s).

The robot performances described here (Section 5) were obtained with an EMD circuit whose main part was implemented on a *Field Programmable Analog Array* (FPAA by Anadigm) conveniently placed off-board [36], except for the results discussed with Fig. 9, which were obtained using the microcontroller-based EMD.

3. Experimental set-up

3.1. Aerial robot

We built a small (100 g) rotorcraft consisting of a rotor, a miniature electronic eye and its control electronics (Fig. 6). This "micro-air vehicle" (MAV) was based on the rotor mast of the Keyence "Revolutor" RC model helicopter. For the sake of experimental convenience, we added a landing gear ($l = 0.3$ m) extending below the robot's eye. The altitude plotted (Section 4) therefore corresponds to z–l, the altitude of the wheels.

3.2. Test-rig

The rotorcraft is tethered to the end of a light, counterbalanced pantographic whirling arm (Fig. 7a) [26,27], which is driven in elevation and azimuth by

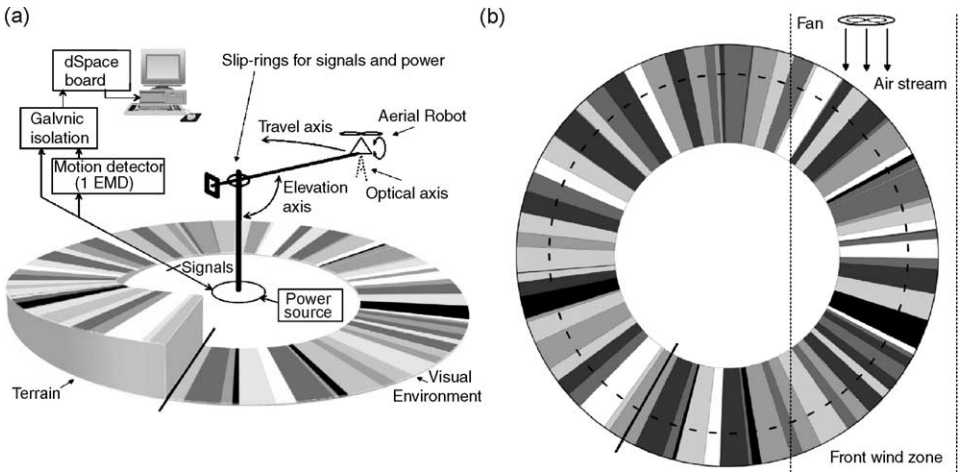

Fig. 7. (a) Test-rig composed of a pantographic whirling arm supporting the 100 g rotorcraft, which flies over an arena with a 4.5 m outside diameter. The richly textured terrain below consists of randomly distributed, variously contrasting sectors (contrast m: $0.04 < m < 0.3$). A ramp covering one third of the arena, which stops abruptly at an altitude of 50 cm, was added to test the robot's terrain following behaviour (Section 4.1). (b) The robot travels above the textured terrain on average along the dotted track with a circumference of 12 m. An electric fan (blade diameter: 0.4 m, blade center height ≈1 m) can blow air to simulate a gust of wind and test the MAV's reaction to wind disturbances.

the aircraft's lift and propulsive forces, respectively. Any increase in the rotor speed (*rpm*) will cause the aerial robot to lift and rise, and any forward tilting of the rotor by a few degrees will cause the robot to move forward (while decreasing the lift slightly).

A computer-printed disc (outer diameter 4.5 m) was laid on the ground to simulate a richly contrasting environment containing randomly ordered contrasting sectors. The various sector widths corresponded to a ∼30-fold spatial frequency range (from 0.06 to 1.75 cycles/°, at $h = 1$ m), which is a suitable range for testing the robustness of the visual processing system. The actual edge contrast m was determined experimentally by measuring the relative luminance (I_1, I_2) of any pair of neighboring sectors and calculating:

$$m = \frac{I_1 - I_2}{I_1 + I_2} \tag{8}$$

The effective edge contrast m measured in the same (near IR) spectral range as that of interest in the robot's eye (the sensitivity of which peaks at $\lambda = 850$ nm), turned out to be relatively low (from 4 to 30%) on the printed disc.

Thus, the visual environment used in this study is much more richly contrasted than natural environments, although it may represent in a cartoon-like fashion the contrast between meadows, cornfields, highways, etc. that meet the eye of a human pilot at high altitudes.

The mean track circumference covered by the MAV during one lap was about 12 m (dotted circle in Fig. 7b). For the sake of convenience, we decided to plot the trajectories (Section 4) on the two dimensional vertical plane defined by the altitude and the horizontal distance traveled.

A PC equipped with an input/output DSP board (dSpace) coupled with MATLAB/Simulink was used to run the experiments in real time (without depending on the PC operating system), while monitoring the robot's behaviour with a pair of ground-truth sensors (a servo-potentiometer on the elevation axis and an optical encoder on the travel axis). The experimenter remotely commanded the servo-motor that pitched the aerial robot forward to attain the required speed.

This test-rig including a tethered MAV enabled us to reliably and reproducibly test the performances of the OCTAVE autopilot under safe flying conditions, while making parameter monitoring simpler.

4. Experimental results

All the experiments shown here were first run in simulation using the very same visual environment as described above, but only the real physical tests are presented here.

4.1. Automatic terrain following

Part of the visual environment was mounted on a slanted surface (a 7° angle "circular ramp", see Fig. 7a). This shallow relief gives rise to a marked output disturbance in the OCTAVE loop (see Fig. 2) and therefore provides a suitable means of testing its efficiency.

The robot's altitude (Fig. 8a) was monitored during 10 cycles of travel over the scene depicted in Fig. 7 and the trajectories recorded showed that the robot automatically followed the terrain smoothly and reproducibly in spite of the presence of aerodynamic disturbances such as ground effects and air turbulence. The OCTAVE autopilot therefore performs reliable terrain following despite the complex dynamics of the overall system (visuomotor system + aeromechanical system + test-rig). The whirling arm gives rise to additional inertia but negligible friction.

The OCTAVE autopilot thus causes the robot's altitude to vary automatically as required by the changing relief of the land. In a detailed study of the trajectories obtained at various ground speeds, we showed [33,34] that an *OF regulation scheme* automatically generates a "safe height", although no explicit knowledge about the ground speed, the descent speed or the height above the ground is available on-board the vehicle. In particular, we established that the robot follows the terrain smoothly at a height which depends on the OF set point ω_{sp}. We observed the fine structure of the OF signal, which the OCTAVE controller attempts to maintain at a constant value. We also established that the "safe height" conveniently increases with the ground speed: the faster the robot is moving, the further away from obstacles it will fly [33,34].

One might argue that the system operates correctly because the richly contrasting sectors of the environment (Fig. 7) provide for sufficient updates of OF

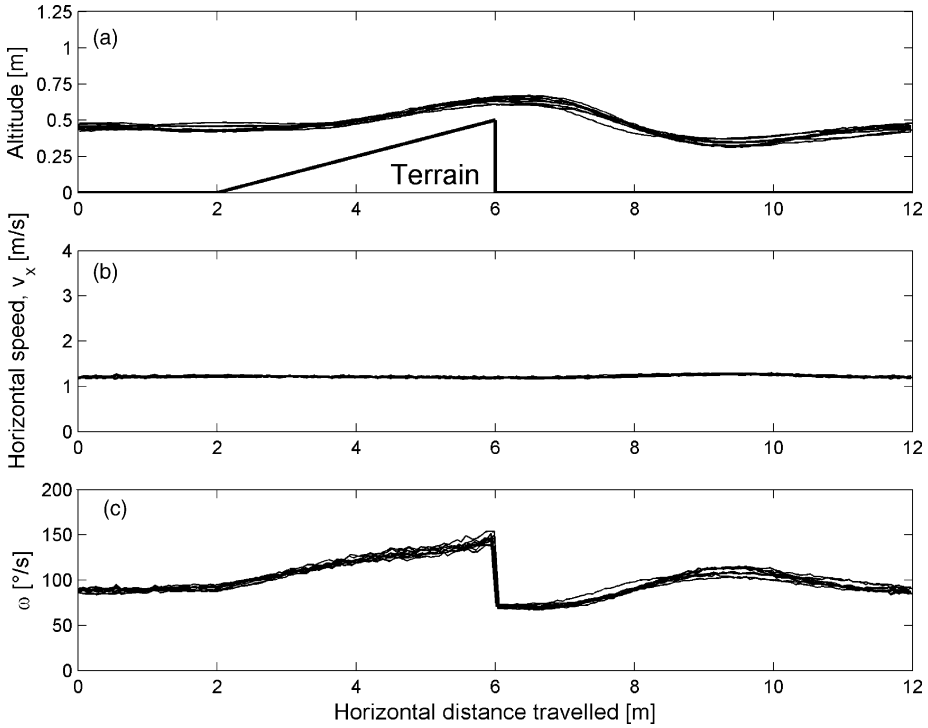

Fig. 8. Automatic terrain following under *optic flow regulation*. This recording shows 10 consecutive trajectories during which the robot covered a distance of 120 m in 100 s at a speed of 1.2 m/s without ever crashing. The optic flow ω generated by the vehicle (c) is disturbed by the presence of the slanted relief. The OF regulation loop rejects this disturbance only partially before re-establishing the steady OF value (about 90°/s) when the ground becomes flat again. The reproducibility of the trajectories (a) attest to the reliability of the OCTAVE autopilot in terrain following tasks.

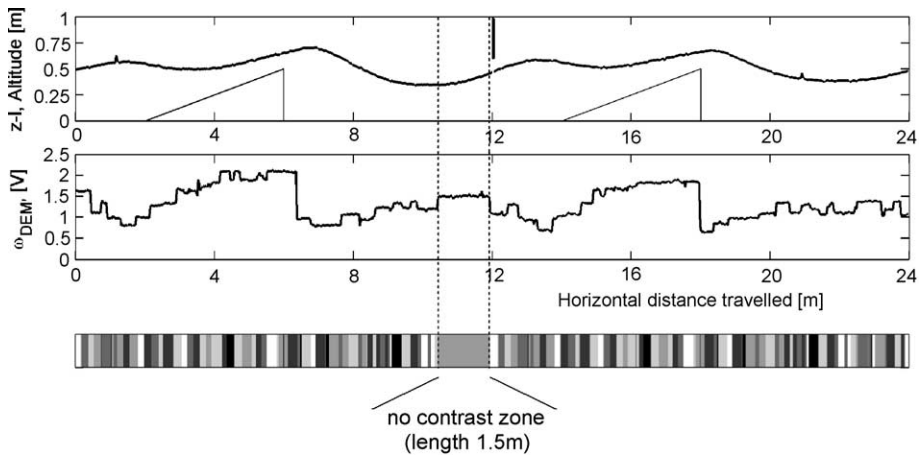

Fig. 9. Effect of a "no contrast zone" on the flight trajectory. Contrast was suppressed over a distance of 1.5 m by covering the ground texture (Fig. 7) momentarily with a 1.5 m long optically uniform cardboard sheet. The latter was retracted once the robot had passed over it and started the second lap.

measurements. Fig. 9 shows the result of an experiment in which we deliberately masked part of the ground texture, by covering it with a 1.5 m long uniform cardboard sheet (region between the two vertical dotted lines in Fig. 9). The ensuing absence of absence of OF measurement during 1 s hardly affected the trajectory. The reason is that the EMD memorized its last OF measurement and the controller kept controlling on the basis of this "old" OF measurement. Obviously, if the "no contrast zone" were longer the robot would easily collide with a rising ground since the OF estimate is not refreshed.

4.2. Automatic take off

In all the subsequent experiments, the ground obstacle (ramp) was removed from the test-rig so that the ground remained flat.

To initiate an automatic take off, the idea was to pitch the rotor axis (i.e., the whole MAV body) "nose down" gradually so as to gradually increase the horizontal speed v_x. The MAV was then expected to take off automatically because the OF controller would keep the ratio v_x/h constant at all times: if v_x increases, h must increase to keep ω constant (Eq. (2)). Fig. 10 shows the results obtained using this strategy. Upon applying a ramp (duration 10 s) to the pitch control, the rotorcraft tilts forward gradually (pitch angle Θ in Fig. 3) until reaching an inclination of 10°. As a result, the ground speed increases gradually (Fig. 10b) and the rotorcraft is bound to gain height (Fig. 10a).

In Fig. 10, five visually guided take off trajectories have been superimposed. The OF regulation loop makes the take off maneuvers highly reproducible. Again, the OCTAVE autopilot proved to be capable of smooth altitude control.

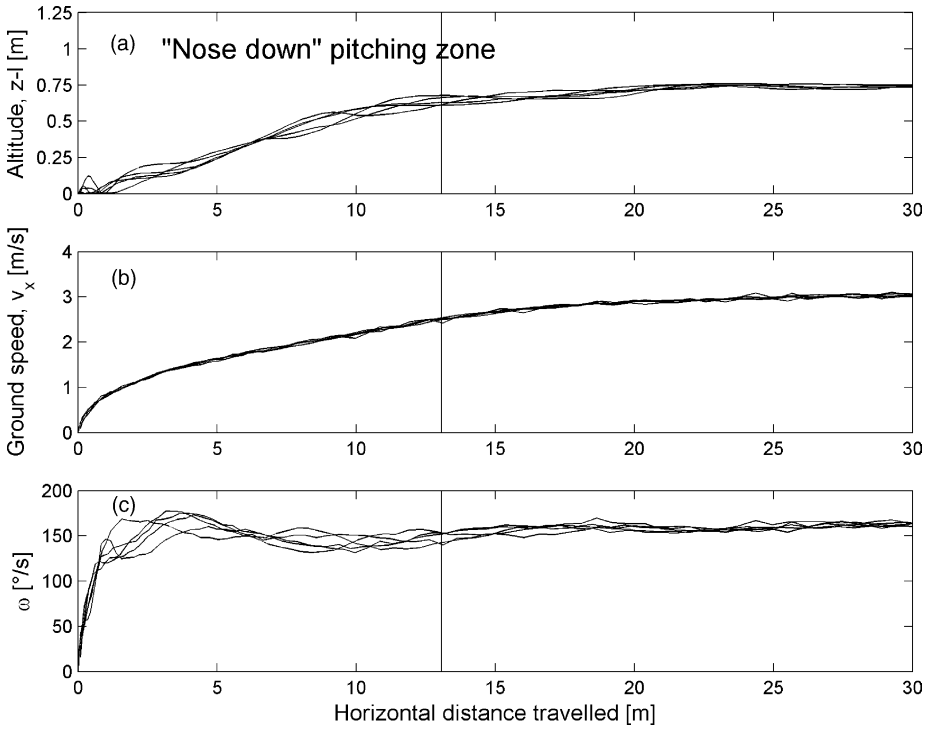

Fig. 10. Automatic take off under visual control. First, the rotor speed is set to the levitation level (see weight compensation bias in Fig. 3) and the OF loop is closed. Within the "nose down pitching zone", the robot is gradually tilted forward and its ground speed therefore increases (b). This results in a smooth and highly reproducible trajectory (a), which is constantly under the firm control of the visual system. The optic flow sensed by the robot (c) is regulated throughout take off up to cruise flight. The OF slightly overshoots at take off before reaching a steady value (about 150°/s). With five tries, the OCTAVE autopilot took reproducible take off trajectories (a).

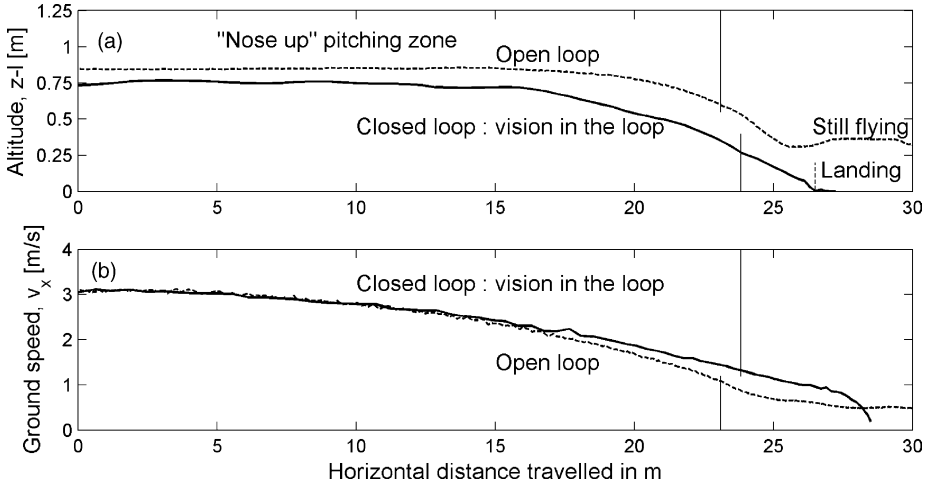

Fig. 11. Automatic landing under visual control. Closed loop (solid line): A gradual rotor tilt "nose-up" triggers automatic landing. The robot decelerates slowly (the inertia of the test-rig slows its deceleration). As the ground speed keeps decreasing (b), the height h over the ground (controlled by the OF autopilot) gradually decreases (a). This eventually results in a smooth landing at a ground speed close to zero. At touchdown, the system switches off the power supply to the rotor. Open loop (dashed line): the system does not succeed in landing because the thrust does not vary.

4.3. Automatic landing

To effect a landing, the idea is to gradually raise the rotorcraft "nose up" so as to gradually decrease the horizontal speed v_x. The OF controller will do the rest, by:

- reducing the height with respect to ground so as to keep the ratio $v_x/h = \omega = \text{constant}$,
- eventually landing the rotorcraft, with a negligible forward speed at touchdown.

Fig. 11a gives the landing trajectories obtained under both closed loop and open loop conditions when the pitch angle Θ (see Fig. 3) was reduced ramp-wise from 10° to 0° (in a 10 s ramp). Under open loop conditions, the MAV has difficulty in landing (Fig. 11b, dashed curve): its lift does not decrease enough because there is no *OF regulation* to pull it downwards. By contrast, the MAV lands smoothly under closed loop conditions (Fig. 11a, solid curve) and smoothly overcomes any ground disturbances.

The five visually guided landing trajectories superimposed in Fig. 12 show that the *OF regulation* makes for reliable and reproducible landing performances. Again, the OCTAVE autopilot always gave a smooth decrease in height. The time required for the robot to land depends on the tilting rate. But it also depends on the travel dynamics between the robot's pitch angle and the ground speed (which includes the test-rig inertia here).

4.4. Automatic reaction to wind disturbances

In the last set of experiments, the course of the rotorcraft was disturbed by a head wind (simulated by a fan, as shown in Fig. 7b) with a speed v_w of up to 1.5 m/s. As shown in Fig. 3, the wind speed constitutes a serious output disturbance, which interferes with the MAV airspeed and alters the ground speed. Under open loop conditions, the robot cannot overcome these output disturbances. Under closed loop conditions, however, a tail wind accelerates the MAV's ground speed and the OCTAVE autopilot reacts by automatically increasing the altitude to maintain the downward OF constant (not shown here).

When encountering a head wind, however, the MAV inevitably loses speed (ground speed). The OCTAVE autopilot will respond in this case so as to automatically decrease the altitude, since it is compelled to maintain the ratio v_x/h constant. This is exactly what is observed experimentally (Fig. 13a and b, dashed lines: light head wind of ∼0.5 m/s).

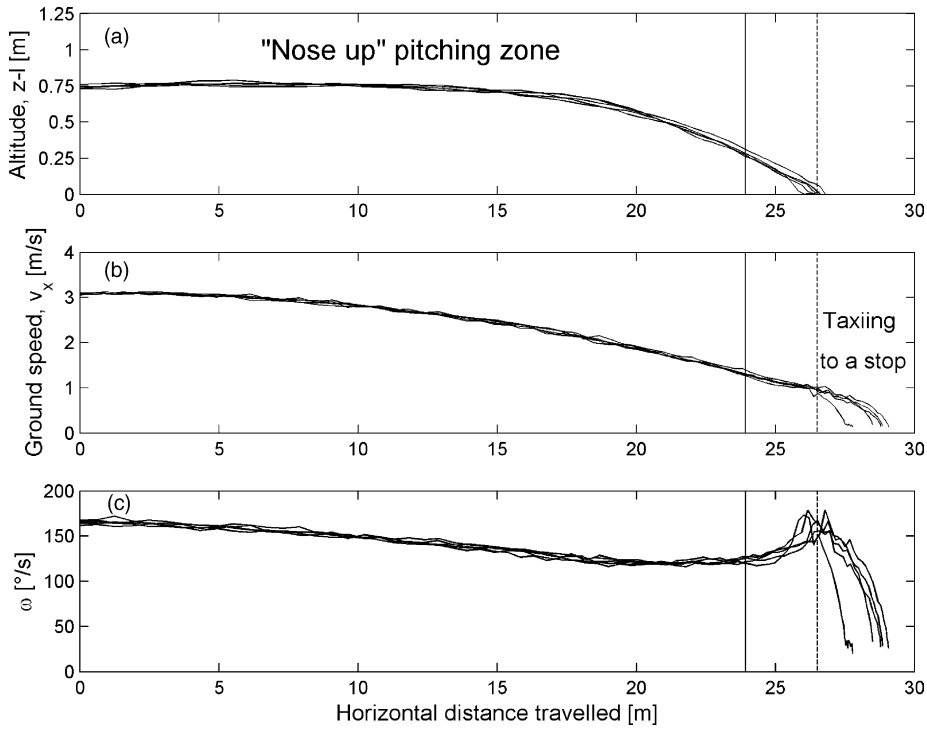

Fig. 12. Automatic landing under visual control. (a) Upon being gradually raised "nose up" in a ramp-like manner (see the "nose up pitching zone"), the miniature rotorcraft is bound to land (five successive landing trajectories are shown superimposed). (b) When the MAV touches the ground, its rotor stops and it taxies to a halt, driven by its own momentum. (c) The *OF regulation loop* attempts to maintain the OF at the set-point value of about 150°/s throughout the descent.

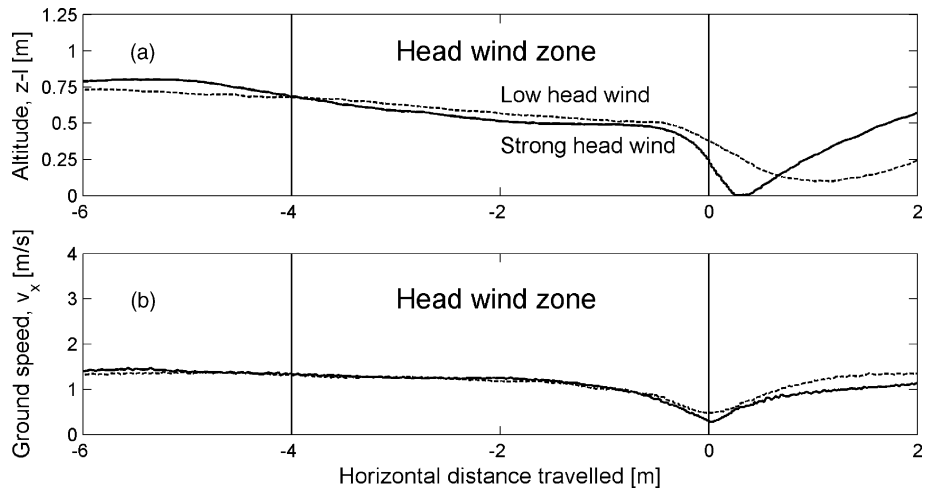

Fig. 13. Coping with a head wind with an *OF regulator* (dashed lines: low head wind $v_w \approx 0.5$ m/s; solid lines: strong head wind $v_w \approx 1.5$ m/s). (b) Head wind can be seen to have reduced the ground speed. (a) The OCTAVE autopilot reacts by automatically decreasing the height of the robot with respect to the ground. The stronger the wind, the lower the aerial minirobot will fly until it alights with negligible forward speed at touchdown (a, solid curves). Since this miniature vehicle does not catch the wind very strongly, we added a 30 cm × 20 cm planar airfoil mounted perpendicular to the travel axis so as to catch the wind better (i.e., to increase the drag) and enhance the effect of the wind.

Upon leaving the wind zone, the MAV is no longer slowed down by the wind. Its ground speed will therefore increase and the OCTAVE autopilot will respond by increasing the altitude again since it cannot help keeping the OF at the set point. This is exactly what is observed experimentally (Fig. 13a and b, dashed lines: light head wind of ∼0.5 m/s).

When facing a strong head wind, the MAV's ground speed decreases so greatly that it tends to zero. This automatically triggers a *forced landing* which is all the safer since the ground speed is so low at touch down (Fig. 13a and b, solid lines: strong head wind of ∼1.5 m/s, landing speed ∼0.3 m/s). A haptic sensor in the landing gear would easily bring the lifting rotor to a halt when the robot alights. This was not done here, however, and the robot is seen to take off again when leaving the wind zone: the robot's height h automatically increases with the ground speed v_x because the OCTAVE *optic flow regulation loop* attempts to maintain the ratio between these two variables constant (Fig. 13a and b, solid lines).

5. Dependence of ground speed and height upon the wind profile

The following discussion assumes that there is no relief so that the altitude z equals the ground height h.

Basically a robot flying at $v_a = v_x$ could fly at any altitude z (i.e., at any point along the vertical line in Fig. 14a). But once equipped with the OCTAVE autopilot, which tend to keep the optic flow ω at a constant value, the robot is bound to fly at an altitude defined by the intersection of the vertical line with the line $z = v_x/\omega$: this is the equilibrium point (black point in Fig. 14). A tail wind (or head wind) will increase (or decrease) the groundspeed, thereby shifting the equilibrium point along the line $z = v_x/\omega$.

We can now take into account the fact that the windspeed increases with the altitude. Up to an altitude of few hundred meters, the wind speed profile $v_w(z)$ is approximately a logarithmic function of the altitude (z) [42]:

$$v_w(z) \approx v_0(\delta) \ln\left(\frac{z}{z_0}\right) \text{ for } z > 10z_0 \quad (9)$$

where δ is the thickness of the surface boundary layer, $z_0 = 0.1$ m in a low density urban zone

hence $z(v_w) = z_0\, e^{v_w/v_0(\delta)}$

Under these conditions, we see (Fig. 14c and d) that the equilibrium point is affected by the dependence of wind speed on altitude.

By head wind (Fig. 14c), the air vehicle remains even closer to the ground (where it is less likely to be disturbed by the head wind). By tail wind, on the other hand, (Fig. 14d), it flies at a higher altitude (where it is more likely to be carried away by the stronger tail wind). Hence, in all cases, the air vehicle behaves suitably by simply remaining locked on to a constant angular ground speed. It automatically rises by tailwind, to an altitude where it meets even better favorable winds. This behaviour is interesting because for a given thrust the air vehicle can travel a greater distance than with classical altitude regulation systems. The air vehicle therefore saves a precious amount of energy.

These reactions can be said to be "ecological" because they are adapted to a natural constraint, according to which the wind speed increases with the altitude.

6. Discussion and conclusion

In this study, we dealt with the reputedly difficult maneuvers that will have to be effected safely by the miniature unmanned aerial vehicles of the future. The OCTAVE autopilot we have described here is a new kind of *automatic flight control system* (AFCS). It is based on a visuomotor control loop that *regulates the optic flow* (OF) measured in the downward direction by acting on the vehicle's lift. The measurement of optic flow is made straight forward by our EMD sensor, which turns out to be a genuine OF sensor. This sensor, oriented downwards, measures neither the ground speed nor the height of flight but the ratio between these two variables in a direct way. We have presented a quantitative study, which shows the validity of this principle. We have described how a miniature (100 g) rotorcraft equipped with the OCTAVE autopilot takes off automatically under visual control, hugs a shallow terrain automatically, lands automatically on command and reacts appropriately to unpredictable head wind

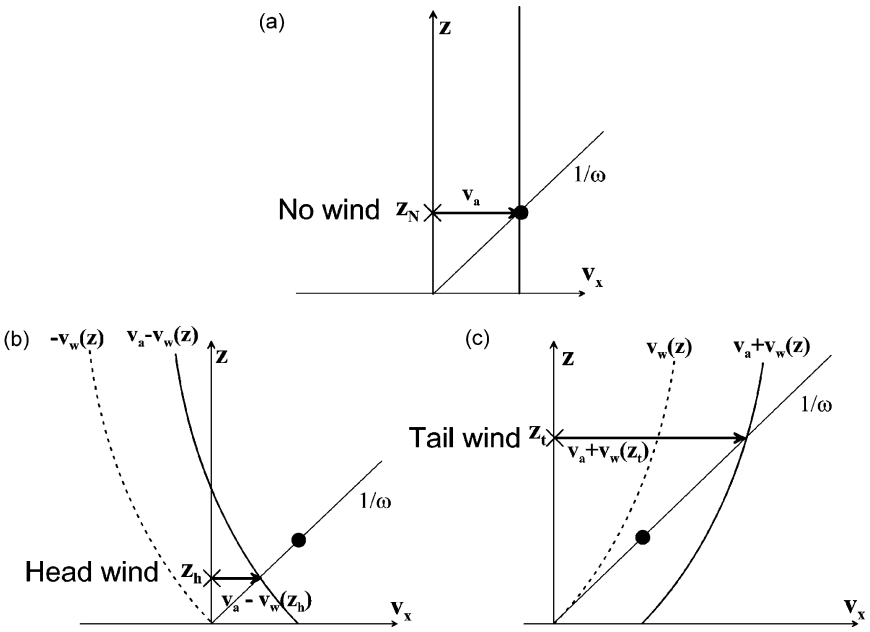

Fig. 14. Speed and altitude equilibrium of an OCTAVE based air vehicle disturbed by wind. (a and b) neglecting and (c and d) taking into account the dependence of wind speed with altitude. For the sake of clarity, we assume the optic flow to be perfectly maintained at the constant value ω despite the disturbances. The straight line $1/\omega$ indicates the set of possible pairs of altitudes and ground speeds allowed in our *optic flow regulation* scheme. (a) In the absence of head wind or tail wind, the ground speed and hence the altitude depend only on the airspeed produced by the vehicle: the vertical line $v_x = v_a$ cuts the line $z(v_x) = v_x/\omega$ at a point which defines the current flight altitude z_N (N for "no wind"). (b) In the presence of a head wind, given that the wind speed increases with the altitude Eq. (9), the ground speed profile ($v_a - v_w(z)$) intersects the straight line $z(v_x) = v_x/\omega$ at a lower altitude than in (a). (c) In the presence of a tail wind, the ground speed profile ($v_a + v_w(z)$) intersects the straight line $z(v_x) = v_x/\omega$ at a greater altitude than in (a).

or tail wind disturbances. The feasibility of OF-based terrain following and landing was originally showed in simulation studies [26]. Another procedure has been proposed to deal with the landing problems [40], which differs from the OF autopilot presented here in that it involves fulfilling two control requirements: (i) "maintaining a constant descent angle" and (ii) "maintaining a constant image angular velocity". The OCTAVE autopilot presented here requires only one *control law*, which consists in *regulating the optic flow by adjusting the thrust*, and a single type of sensor which is an optic flow sensor. In our *optic flow regulation loop*, the controller adjusts only the thrust amplitude, regardless of the vehicle's current forward groundspeed, airspeed or descent speed. As we have shown here, this simple OF *regulation loop* suffices to generate many interesting behaviours.

First, reliable terrain-following performances were obtained: OCTAVE suitably copes with the "disturbances" caused by a slanted ground by performing *terrain following*. The OCTAVE AFCS turned out to be robust and efficient within a given range of forward speeds (1–3 m/s). A "safe height" is generated automatically, which increases most appropriately with the ground speed [33,34]. We then described how the trajectory of the MAV in the vertical plane can be changed by simply altering the pitch angle, which determines the ground speed. Pitching the robot gradually "nose-down" and thus increasing its ground speed causes the robot to automatically take off. Conversely, raising the robot gradually backwards ("nose up") causes it to lose height automatically until it eventually alights with negligible speed at touchdown. These apparently complex maneuvers are therefore performed automatically in response to simple pitch commands.

When entering a head wind zone, the robot automatically reacts by flying lower: it reduces its height

h above the ground, thus maintaining a "safe height" that suitably matches its speed v_x, so as to keep the ratio between them constant. This reaction (which might be problematic in the case of a passenger aircraft, but may be tolerable in UAVs and MAVs, depending on their mission) actually occurs in nature. Reactions of this kind are typical of both insects and birds. Migrating insects [22] and migrating birds [1] typically ascend under tail winds and descend when a lull occurs or when they come to face a light head wind. Whether it occurs in insects or birds or MAVs, this behaviour is all the more appropriate and ecological since a descending reaction to a head wind will bring them to lower altitudes where less stronger winds prevail, leading to valuable energy savings during their migratory (in the case of insects and birds) or survey flights (in the case of MAVs). Conversely, an ascending reaction to a tail wind will bring them to higher altitudes where even more favorable winds prevail.

Unlike most of the autopilots classically used in manned helicopters, the OCTAVE autopilot was not designed to provide the aerial robot with height holding or ground speed holding skills. It ensures that "OF holding" occurs so that the MAV will reach a "safe height" automatically at any ground speed. The main advantage of the OCTAVE autopilot is that it ensures that any maneuvers and disturbance rejection (terrain relief, wind) will occur at all costs without colliding with the ground: the result is measured in terms of task performances, and not in terms of the metric variables (airspeed, height, descent speed, etc.) usually measured on-board aircraft. The robot is able to take off, follow a shallow terrain, land and react to wind disturbances *although it is completely unaware of its airspeed, groundspeed, descent speed, its descent angle, its height over the terrain or its absolute altitude at any time*. In contrast with the OCTAVE autopilot, classical AFCS are designed, for example, with altitude holding or speed holding capabilities in mind and they usually operate far from the ground. Automatic landing systems classically require off-board and bulky ground station instrument landing system (ILS) equipment. In the case of UAVs, they include items such as a radar station able to track the aircraft during its descent.

The use of a tether was essential here to be able to implement and test the basic strategy used: *OF regulation* on an elementary rotorcraft with limited (three) degrees of freedom. Quantitative tests on free-flying MAVs are more difficult to carry out and lack reproducibility [5,6,16] because a MAV is unlikely to fly twice at the same height over the same site under the same wind disturbance conditions. In our quantitative tests, however, the whirling arm introduced undesirable inertia into the control loop, which adversely affected both the heave and the surge dynamics: the robot was less agile than it would have been if it were flying freely. On the other hand, a supporting tether facilitates the parameter monitoring, and the understanding and tuning of the perception/action loop, while making the experiments highly reproducible (see Figs. 8, 10 and 12). For these reasons, we decided to use a step-by-step approach starting with a tethered vehicle to test the fundamentals of the OCTAVE principle.

The system we have described here for the visual guidance of an aerial vehicle was inspired by the insect world, and the visual processing system itself was also inspired by the results of electrophysiological experiments carried out on living insects. Most present-day computer-assisted visual systems are not up to the task of guiding a micro-air vehicle weighing less than 100 g, which would entail reducing the total avionic payload to less than 10 g. Biologically inspired robotics can provide MAVs with well tried and tested alternative solutions, which in some cases are also scalable to larger UAVs. The stealth OCTAVE autopilot requires remarkably few resources. Its simple principle suggests that we are working towards a *generic solution* to reputedly complex guidance problems which, as we have shown here, can be solved by one and the same *OF regulation loop*. Once it has been further developed, and its field of view enlarged in particular, the OCTAVE autopilot promises to provide MAVs, UAVs and full-sized aircraft with greater decision-making autonomy. It can also be used to warn pilots about imminent risks of collision with the terrain, while automatically preventing controlled flight into terrain.

In a near future, the OCTAVE autopilot will be implemented on-board free-flying 100 g MAV. The body roll, the body pitch and the eye pitch counter-rotation will be servoed using a micro vertical gyro. The controller parameters will be modified to take into account the faster dynamics of the free flying robot. The overall structure of the OCTAVE autopilot described in this

paper will, however, remain the same. The number of EMD will be increased to enlarge the field of view and cope with the sparser textures found in natural environment.

Since automatic take off, terrain following, ground collision avoidance and landing are also major issues for planetary [24,29] and submarine operations [9,11], the vision-based OCTAVE autopilot could also potentially be adapted to spacecraft, planetary vehicles, and benthic submarines (equipped with projectors to create contrast). As regards benthic navigation of a submarine vehicle, Eq. (9) is a function derived from the Navier-Stokes equation that also applies to liquid environments. The OCTAVE system might therefore provide a suitable means of making autonomous underwater vehicles (AUVs) able to navigate automatically at a safe height above the sea bottom without having to explicitly measure their height, their depth and the water stream velocity.

Patent

A patent on the optic flow based OCTAVE autopilot was published on March 19, 2004 (WO2004025386).

Acknowledgements

We thank S. Viollet for his fruitful comments and suggestions during this work, S. Durand from Galatée Films for his data about bird migration, J. Serres for his comments on the manuscript, S. Amic for the design of the EMD circuit combining analog and digital processing, M. Boyron for his outstanding technical assistance, M. Rigal for the galvanic isolation of the dSpace board and J. Blanc for improving the English manuscript. This research was supported by CNRS (Life Science, Engineering Science, Communication and Information Science and Technology, Cogniscience, Microsystem and Microrobotic Programmes) and by an EU contract (IST/FET – 1999 – 29043).

References

[1] T. Alestram, Bird Migration, Cambridge University Press, 1990.

[2] O. Amidi, T. Kanade, J.R. Miller, Vision-based autonomous helicopter research at Carnegie Mellon Robotics Institute 1991–1997, in: Proceedings of the American Helicopter Society Int. Conf. Gifu, Japan, 1998.

[3] C. Blanes, Appareil visuel élémentaire pour la navigation à vue d'un robot mobile autonome, Master Thesis in Neurosciences ("DEA" in French), Neurosciences, Univ. Aix-Marseille II, 1986.

[4] C. Blanes, Guidage visuel d'un robot mobile autonome d'inspiration bionique, PhD Thesis, Spécialité: Signal, Image, Parole, Institut National Polytechnique de Grenoble, 1991.

[5] G.L. Barrows, C. Neely, K.T. Miller, Optic flow sensors for MAV navigation, in: Fixed and flapping wing aerodynamics for Micro Air Vehicle applications, Progress in Astronautics and Aeronautics, AIAA, 2001. Vol. 195, 557–574.

[6] J.S. Chahl, M.V. Srinivasan, S.W. Zhang, Landing Strategies in Honeybees and Applications to Uninhabited Airborne Vehicles, Int. J. Robot. Res. 23 (2) (2004) 101–110.

[7] J.S. Chahl, S. Thakoor, N. Le Bouffant, G. Stange, M.V. Srinivasan, B. Hine, S. Zornetzer, Bioinspired engineering of exploration systems: a horizon sensor/attitude reference system based on the dragonfly ocelli for Mars Exploration Applications, J. Robot. Sys. 20 (1) (2003) 35–42.

[8] T. Collett, H. Nallbach, H. Wagner, Visual stabilization in arthropods, in: F.A. Miles, J. Wallman (Eds.), Visual Motion and Its Use in the Stabilization of Gaze, Elsevier, 1993, pp. 239–263.

[9] V. Creuze, B. Jouvencel, Avoidance of underwater cliffs for autonomous underwater vehicles, in: Proceedings of the IEEE Conf. on Intelligent Robots and Systems (IROS), Lausanne, Switzerland, 2002, pp. 793–798.

[10] C.T. David, The relationship between body angle and flight speed in free-flying Drosophila, Physiol. Entomol. 3 (1978) 191–195.

[11] M. Dunbabin, P. Corke, G. Buskey, Low-cost vision-based AUV Guidance system for reef navigation, in: Proceeding of IEEE International Conference on Robotics and Automation (ICRA 2004), New Orleans, USA, pp. 7–12.

[12] N. Franceschini, C. Blanes, L. Oufar, Passive, non-contact optical velocity sensor (in French), Dossier technique ANVAR/DVAR N°51549, Paris, 1986.

[13] N. Franceschini, J.M. Pichon, C. Blanes, From insect vision to robot vision, Philos. Trans. Royal Soc. Lond. Ser. B 337 (1992) 283–294.

[14] N. Franceschini, A. Riehle, A. Le Nestour, Directionally selective motion detection by insect neurons, in: D.G. Stavenga, R.C. Hardie (Eds.), Facets of Vision, Springer, Berlin, 1989, pp. 360–390.

[15] S. Furst, S. Werner, D. Dickmanns, S. Werner, Landmark navigation and autonomous landing approach with obstacle detection for aircraft, in: Proceedings of SPIE AeroSense '97 Conf., Vol. 3088, Orlando FL, 1997, pp. 94–105.

[16] W.E. Green, P.Y. Oh, G. Barrows, Flying insect inspired vision for autonomous aerial robot maneuvers in near-earth environments, in: Proceeding of IEEE International Conference

of Robotics and Automation (ICRA), New Orleans, 2004, pp. 2347–2352.
[17] R.R. Harrison, C. Koch, A robust analog VLSI motion sensor based on the visual system of the fly, Autonomous Robots 7 (1999) 211–224.
[18] K. Hausen, M. Egelhaaf, Neural mechanisms of visual course-control in insects, in: D.G. Stavenga, R.C. Hardie (Eds.), Facets of Vision, Springer, Berlin, 1989, pp. 391–424.
[19] M. Ichikawa, H. Yamada, J. Takeuchi, Flying robot with biologically inspired vision, J. Robot. Mechatron. 13 (2001) 621–624.
[20] B. Kadmiry, P. Bergsten, Pr. D. Driankov, Autonomous helicopter using fuzzy-gain scheduling, in: Proceedings of the IEEE Int. Conf. on Robotic and Automation (ICRA 2001), vol. 3, Seoul, Korea, 2001, pp. 2980–2985.
[21] J.S. Kennedy, The visual response of flying mosquitoes, Proc. Royal Soc. Lond. Ser. A 109 (1939) 221–242.
[22] J.S. Kennedy, The migration of the desert locust (*Schistocerca gregaria* Forsk.), Philos. Trans. Royal Soc. Lond. Ser. B 235 (1951) 163–290.
[23] J. Kramer, R. Sarpeshkar, C. Koch, Pulse-based analog VLSI velocity sensors, IEEE Trans. Circuits Sys. II 44 (1997) 86–101.
[24] T. Kubota, T. Hashimoto, J. Kawaguchi, Image processing for asteroid exploration mission MUSES-C, in: Proceedings of the IEEE 11th Int. Conf. on Advanced Robotics (ICAR), Coimbra, Portugal, 2003, pp. 1221–1226.
[25] F. Mura, N. Franceschini, Visual control of altitude and speed in a flying agent, in: D. Cliff, et al. (Eds.), From Animals to Animats III, MIT Press, Cambridge, USA, 1994, pp. 91–99.
[26] T. Netter, N. Franceschini, Neuromorphic optical flow sensing for nap-of-the-earth flight, in: D.W. Gage, H.M. Choset (Eds.), Proceedings of the SPIE Conf. on Mobile Robots XIV, Bellingham, USA, 1999. SPIE vol. 3838, pp. 208–216.
[27] T. Netter, N. Franceschini, A robotic aircraft that follows terrain using a neuromorphic eye, in: Proceedings of the IEEE Conf. on Intelligent Robots and Systems (IROS), Lausanne, Switzerland, 2002, pp. 129–134.
[28] T.R. Neumann, H. Bülthoff, Insect inspired visual control of translatory flight, in: Proceedings of the ECAL 2001. Springer, Berlin, 2001, pp. 627–636.
[29] G. Paar, W. Pölzleitner, Descent and landing phase: vision based robust spacecraft motion estimation and elevation modeling, in: CNES (Eds.), Missions, Technologies and Design of Planetary Mobile Vehicles, Cépaduès-éditions, Toulouse, France, 1992, pp. 259–272.
[30] J.-M. Pichon, C. Blanes, N. Franceschini, Visual guidance of a mobile robot equipped with a network of self-motion sensors, in: W.J. Wolfe, W.H., Chun (Eds.), Proceedings of the SPIE Conf. on Mobile Robots IV, Bellingham, USA, 1989. SPIE vol. 1195, pp. 44–53.
[31] W. Reichardt, Movement perception in insects, in: W. Reichardt (Ed.), Processing of Optical Data by Organisms and by Machines, Academic Press, New York, 1969, pp. 465–493.
[32] J.M. Roberts, P.I. Corke, G. Buskey, Low-cost flight control system for a small autonomous helicopter, in: Proceedings of the 2002 Australasian Conference of Robotics and Automation, 2002, pp. 71–76.
[33] F. Ruffier, N. Franceschini, OCTAVE, système de contrôle bio-inspiré de l'altitude d'un micro-aéronef, in: Actes des 1ères journées du Réseau Thématique Pluridisciplinaire Micro-robotique, CNRS, Rennes, France, November 2002.
[34] F. Ruffier, N. Franceschini, OCTAVE, a bioinspired visuo-motor control system for the guidance of Micro-Air Vehicles, in: A. Rodriguez-Vazquez, D. Abbott, R. Carmona (Eds.), Bioengineered and Bioinspired Systems, Bellingham, USA, May 2003. SPIE vol. 5119, pp. 1–12.
[35] F. Ruffier, N. Franceschini, Visually guided micro-aerial vehicle : automatic take off, terrain following, landing and wind reaction, in: Proceeding of the IEEE International Conference on Robotics and Automation (ICRA 2004), New Orleans, USA, April 2004, pp. 2339–2346.
[36] F. Ruffier, S. Viollet, S. Amic, N. Franceschini, Bio-inspired optical flow circuits for the visual guidance of micro-air vehicles, in: Proceedings of the IEEE Int. Symposium on Circuits and Systems (ISCAS), vol. III, Bangkok, Thailand, May 2003, pp. 846–849.
[37] F. Ruffier, S. Viollet, N. Franceschini, Visual control of two aerial mini-robots by insect-based autopilots, Advanced Robotics 18 (2004) 771–786.
[38] K. Schutte, H. Sahli, D. Schrottmayer, M. Eisl, F.J. Varas, M. Bajic, M. Uppsall, E. den Breejen, ARC: a camcopter based mine field detection system, in: Proceedings of the Fifth International Airborne Remote Sensing Conference, San Francisco, 2001.
[39] C.S. Sharp, O. Shakernia, S.S. Sastry, A vision system for landing an unmanned aerial vehicle, in: Proceedings of the IEEE Int. Conf. on Robotics and Automation (ICRA), Seoul, Korea, 2001, pp. 1720–1727.
[40] M.V. Srinivasan, S.W. Zhang, J. Chahl, E. Barth, S. Venkatesh, How honeybees make grazing landings on flat surfaces, Biological Cybernetics 83 (3) (2000) 171–183.
[41] M.V. Srinivasan, S.W. Zhang, M. Lehrer, T.S. Collett, Honeybee navigation *en route* to the goal: visual flight control and odometry, J. Exp. Biol. 199 (1996) 237–244.
[42] H. Tennekes, A model for the dynamics of the inversion above a convective boundary layer, J. Atmos. Sci. 30 (1973) 558–567.
[43] S. Viollet, N. Franceschini, Super-accurate visual control of an aerial minirobot, in: U. Rückert, J. Sitte, U. Witkowski (Eds.), Proceedings of the Autonomous Minirobots for Research, Edutainment AMIRE, Paderborn, Germany, 2001, pp. 215–224.
[44] S. Viollet, N. Franceschini, A miniature biomimetic gaze control system, in: Proceedings of the IEEE International Conference on Robotics and Automation (ICRA 2004), New Orleans, USA, pp. 504–510.
[45] W.C. Wu, L. Schenato, R. J. Wood, R.S. Fearing, biomimetic sensor suite for flight control of a micromechanical flying insect: design and experimental results, in: Proceedings of the IEEE

Int. Conf. on Robotics and Automation (ICRA), Taipei, Taiwan, 2003, pp. 1146–1151.

Franck Ruffier was born in Villefranche-sur-Saône, France. He got an engineering degree in Computer Sciences, Electronics and Control Theory from the National Polytechnic Institute, Grenoble. He spent 1 year as exchange student in the Automatic Control department in Lund, Sweden. In 2000, he joined the CNRS Biorobotic Research Group in Marseille, France, as a Ph.D. student and received the Ph.D. degree from the National Polytechnic Institute, Grenoble (INPG) in September 2004.

Nicolas Franceschini was born in Mâcon, France. He graduated in Electronics and Control Theory from the National Polytechnic Institute, Grenoble and then studied Biophysics and Neurophysiology at the University and Max-Planck Institute for Biological Cybernetics, Tübingen (Germany). He received the doctor degree from the National Polytechnic Institute in Grenoble in 1972 and spent 9 years as a researcher at the Max-Planck Institute. He then settled down in Marseille, where he built up the Neurocybernetics Research Group at the National Center for Scientific Research (C.N.R.S.). His present position is C.N.R.S Research Director and Head of the Biorobotic Research Group at CNRS/Univ de la Méditerranée, Marseille, France.